WEP Warwick Evans Publishing

International Journal of Materials Science and Technology Studies

ISSN: 3006-7693 (Print), ISSN: 3006-3744 (Online) | Volume 5, Number 2, Year 2026
DOI: https://doi.org/10.62051/ijmsts.v5n2.08
Journal homepage: https://wepub.org/index.php/IJMSTS/index

Forming Mechanism of Hydrogel Sensors Based on Hollow Fiber with Heteromorphic Lumen

Yu Li *, Shengzhao Qiao

School of Mechanical and Power Engineering, Henan Polytechnic University, Jiaozuo, Henan, 454000, China

*Corresponding Author: Liyu@hpu.edu.cn

ABSTRACT

Cross-linking reaction flow forming is an advanced technology for preparing hollow fiber hydrogels, featuring simple process, continuous meter-level preparation and 3D structure construction. However, hydrogel sensors made by this method have poor tunability in mechanical and electrical properties, limiting their application. To solve this, this study focuses on the design, preparation, performance testing of heteromorphic lumen hydrogel sensors and their application in flexible sensors. Firstly, an experimental platform for precise extrusion control was built using a coaxial nozzle and microinjection pump system. By adjusting the flow rate of inner-phase calcium chloride (with outer-phase sodium alginate), variable-diameter heteromorphic lumen hydrogels were precisely prepared. A theoretical model based on flow rate regulation was proposed to characterize lumen morphology changes, providing theoretical support for structural optimization. Subsequently, the effects of sodium alginate (3%–5%) and lithium chloride (3%–5%) concentrations on hydrogel properties were explored. Results show that higher sodium alginate concentration improves tensile strength, elongation at break and fatigue resistance, while electrical properties first rise then fall. Higher lithium chloride concentration reduces mechanical properties but enhances electrical conductivity (with significant strain-dependent changes). The optimal formulation (3.75% sodium alginate, 5% lithium chloride) achieves 65 kPa maximum stress and 33.86 S/m maximum conductivity. In summary, this study realized precise regulation and performance optimization of hydrogel sensors via heteromorphic lumen design. Flow rate adjustment and concentration optimization are crucial for improving their mechanical, electrical and sensing properties, providing theoretical and practical support for their application in high-precision biological signal monitoring and flexible electronics.

KEYWORDS

Hollow fiber; Special-shaped lumen; Flow rate change; Preparation and regulation; Flexible sensor

1. INTRODUCTION

The coaxial reaction flow method [1] is widely used in microfluidics and chemical reactions for preparing hollow-structured materials, with broad applications in tissue engineering and bioprinting. Based on a coaxial nozzle, this method enables two or more fluids to flow along the same central axis through different channels (inner fluid as core, outer fluid as peripheral material); upon extrusion, the fluids form tubular or hollow fiber structures via cross-linking reactions. For instance, the outer cross-linkable hydrogel (e.g., sodium alginate) rapidly solidifies into calcium alginate hydrogel through ionic cross-linking with the inner cross-linking agent (e.g., calcium chloride), making it suitable for preparing hollow biomedical structures like blood vessels and nerve catheters.

Axially uniform hollow fibers [1-4] are expected to be transformed into complex-shaped hollow hydrogel structures for advanced biomedical applications [5-6], but this requires sophisticated equipment. Examples include centrifugal microfluidic systems (controlling hydrogel microfiber geometry via nozzle structure, solution properties, and centrifugal conditions [7]), newly developed microfluidic spinning devices (preparing necklace-like microfibers [8]), and the rope-coil effect (mass-producing microfibers with spiral channels via coaxial microfluidics [9]). Hollow hydrogel sensors with diverse core morphologies are a research focus, as they enhance mechanical properties, adaptability, and electrical performance.

Numerous studies have advanced complex hollow hydrogel preparation via improved coaxial or microfluidic methods. Wu et al. [10] proposed a supramolecular interaction-based method using gelatin microspheres as core templates, which cross-link with sodium alginate via Ca^{2+} diffusion to form a hydrogel shell; dissolving the gelatin core yields hollow structures, with flexible regulation of morphology and mechanical properties. Liang et al. [11-12] developed a non-coaxial microfluidic device for preparing complex-shaped hollow microfibers (e.g., helical, necklace-like) without coaxial nozzles, adjusting fiber size via flow rate. Jia et al. [13] and Rui et al. [14] proposed a one-step microfluidic method for complex spiral microfibers, controlling pitch and amplitude via flow rate and viscosity; Rui et al. [15] further prepared magnetically responsive spiral microfibers by adding magnetic nanoparticles.

Advances in printing/spinning technologies have expanded hollow hydrogel applications. Zhang et al. [16-17] developed a pressure-assisted 3D printing platform with coaxial microfluidic channels for printing hollow hydrogel fibers. Hua et al. [18] prepared highly anisotropic polyvinyl alcohol hydrogels via direct-write printing, with superior mechanical properties. The Ozbolat group [18] realized coaxial blood vessel printing using a self-made needle, with 4% sodium alginate (outer) and 4% calcium chloride (cross-linking agent), yielding hydrogel tubes with inner diameter (135±13) μm and outer diameter (309±22) μm.

In summary, direct-write 3D printing combined with coaxial reaction flow provides an efficient, controllable method for hollow hydrogel preparation: coaxial nozzles enable synchronous extrusion of inner/outer fluids, with the outer hydrogel rapidly solidifying upon contact with the inner cross-linking agent. However, traditional coaxial methods mostly produce axially uniform hollow fibers, limiting the controllable preparation of irregular cavity structures. Additionally, relevant studies lack in-depth discussion on structure formation mechanisms, expansion to complex irregular cavities, and further application research in functional devices such as sensors.

2. FORMING PRINCIPLE AND DEVICE OF HETEROMORPHIC LUMEN HYDROGEL SENSOR

The forming principle and device of the heteromorphic lumen hydrogel sensor are shown in Fig. 1. The core solution (Ca^{2+}) diffuses bilaterally and undergoes a cross-linking reaction with the shell solution; as the co-flow distance increases, the shell sol is cross-linked and fixed into a gel, generating hollow fibers. Fig. 1b presents the coaxial nozzle used in this study, improved from the traditional flush inner-outer needle coaxial nozzle: the outer needle is extended to confine the coaxial fluid's diffusion reaction stage (reaction flow) in a more controllable laminar flow space, and a transparent polytetrafluoroethylene (PTFE) tube is adopted as the outer needle for online observation of the reaction process; meanwhile, the inner needle has a semi-flexible structure with dynamic coaxiality optimization, ensuring more uniform wall thickness of the prepared hollow fibers.

During extrusion, calcium ions (Ca^{2+}) from the calcium chloride solution undergo a coordination reaction with carboxyl groups ($–COO^-$) in sodium alginate to form a cross-linked structure. The reaction rate is mainly affected by calcium chloride flow rate: at low flow rates, cross-linking is relatively slow, forming a gradual cross-linked layer that constrains the inner and outer lumen fluids,

leading to gradual lumen shrinkage and stabilization. With increasing flow rate, cross-linking accelerates, increasing hydrogel formation rate and further affecting the hydrogel lumen's morphology and diameter.

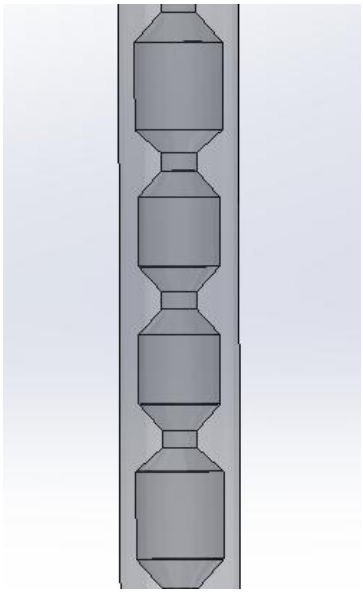

Figure 1. Theoretical Model of Variable-Diameter Hydrogel

2.1. Reaction Kinetics Model of the Cross-Linking Process

During the cross-linking process, the diffusion and reaction rate of Ca^{2+} are mainly affected by the change of flow rate, and this process can be described by a diffusion-reaction model. According to Fick's law, the diffusion rate of Ca^{2+} in the calcium chloride solution can be expressed as:

$$J = -D\frac{dC}{dx} \tag{1}$$

J represents the diffusion flux of Ca^{2+}, D is the diffusion coefficient, and dC/dX denotes the concentration gradient.

Similarly, the cross-linking reaction rate can be described by the following equation:

$$r = kC_{Ca^{2+}}[COO^{-}] \tag{2}$$

Where r is the cross-linking reaction rate, $C_{Ca}{}^{2+}$ is the concentration of Ca^{2+}, $[COO^{-}]$ represents the concentration of free carboxyl groups in sodium alginate, and k denotes the reaction rate constant.

2.2. Geometric Model of Variable-Diameter Lumens

Based on the geometric characteristics of the hydrogel lumens, they maintain a cylindrical shape during the preparation process, and their diameter can be influenced by variations in the flow rate. It is assumed that the temporal evolution of the lumen diameter can be approximately described by the following equation:

$$d(t) = d_0 + \Delta d(t) \tag{3}$$

Where d_0 is the initial lumen diameter of the hydrogel, and $\Delta d(t)$ represents the influence of flow rate variation on the lumen diameter.

Δd(t) increases with an increasing flow rate and decreases as the flow rate declines.

2.3. Theoretical Model for the Formation of Hydrogels with Irregular Lumens

Combining the Hagen–Poiseuille equation with key parameters including the critical relative velocity, critical sol layer thickness, and critical viscosity, the theoretical formation model for variable-diameter hydrogels can be established as follows:

$$d(t) = \frac{d_0}{1+\alpha \cdot Q_{\text{inner}} \cdot \eta} \tag{4}$$

d(t) is the time-dependent function of the lumen diameter;

d_0 denotes the initial lumen diameter;

α represents the influence coefficient of flow rate and solution viscosity on lumen morphology;

Qinner is the flow rate of the internal phase;

η stands for the viscosity of the solution.

As depicted in Figure 1, under the condition of constant solution viscosity, the lumen formation process can be precisely regulated by adjusting the internal and external flow rates of the solution, thereby realizing the controllable preparation of variable-diameter hydrogels.

3. EXPERIMENTS AND CHARACTERIZATIONS

3.1. Materials and Instruments

Sodium alginate (NaAlg, chemically pure, CP) was purchased from Sinopharm Chemical Reagent Co., Ltd.

Anhydrous calcium chloride ($CaCl_2$, analytical reagent grade, AR) was obtained from Sinopharm Chemical Reagent Co., Ltd.

Murexide (ammonium purpurate) was supplied by Damao Chemical Reagent Factory, Tianjin.

Fixed amounts of NaAlg powder and murexide tracer were weighed using an electronic balance and dissolved in deionized water to prepare NaAlg solutions with concentrations of 3 wt%, 3.5 wt%, 4 wt%, and 4.5 wt%, respectively.

The mixtures were stirred at room temperature for 10 h at a rotation speed of 120 $r \cdot min^{-1}$ using a thermostatic magnetic stirrer, followed by additional stirring for 3 h, and then allowed to stand for 6 h to remove air bubbles.

$CaCl_2$ solutions with different concentrations (1 wt%, 3 wt%, 5 wt%, 7 wt%) were prepared in the same manner.

The main experimental instruments included: electronic balance (AB104-N, Puchun Metrological Instrument Co., Ltd., Shanghai); thermostatic magnetic stirrer (H01-1B, Meiyingpu Instrument Co., Ltd., Shanghai); industrial microscope (BC4800, Bocheng Electronic Technology Co., Ltd.); and microfluidic syringe pump (XMSP-1C, Nanjing Ximai Nano Technology Co., Ltd.).

3.2. Construction of the Experimental Platform

The overall setup of the experimental platform is illustrated in Figure 2, which consists of a split-type digital microinjection pump, an industrial microscope, a 3D printer, and other supporting devices. During the experiment, the industrial microscope is mounted horizontally on a lifting stage, and

focusing is achieved by adjusting the height of the stage. The extrusion of fluids is controlled by the split-type digital microinjection pump, with two independent syringe pumps used to regulate the flow rates of sodium alginate sol (shell layer) and calcium chloride solution (core layer), respectively. Considering that the flexible tubing undergoes elastic deformation under internal fluid pressure, the microinjection pumps are fixed on the platform, and the tubing length is minimized to reduce such deformation. The extrusion rate and flow rate of the microinjection pumps can be adjusted via a control card, while the flow behavior of calcium chloride solution inside the coaxial nozzle is monitored in real time using the industrial microscope.

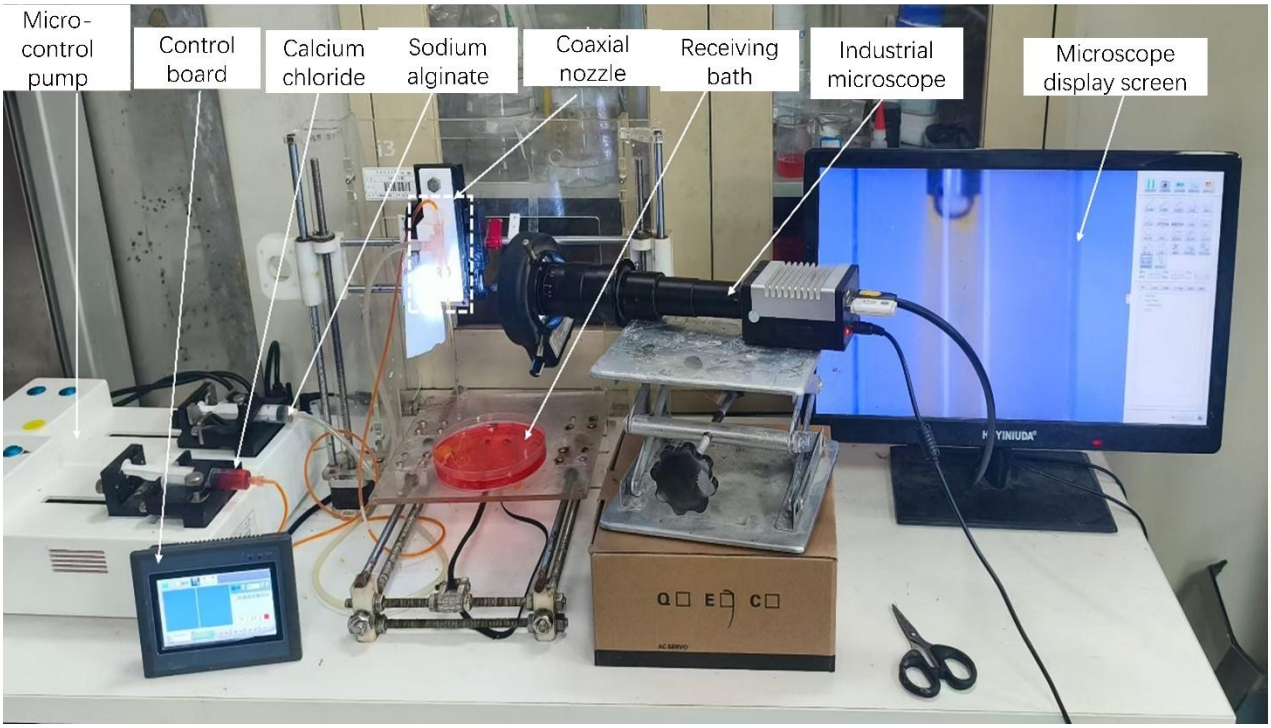

Figure 2. General Assembly of the Experimental Platform for Heterotypic Lumen Hollow Fibers

3.3. Preparation of Heterotypic Lumens

In this experiment, the preparation of hydrogel fibers was accomplished using the constructed printing platform. The established experimental platform employed a coaxial extrusion nozzle with an inner needle diameter of 1.6 mm and an outer needle diameter of 3 mm, ensuring the accurate distribution and control of the inner and outer phase solutions. The inner phase was a 3% calcium chloride solution, and its extrusion rate varied according to the preset flow rate rule, increasing from 0.6 mL/min to 1.1 mL/min and then decreasing back to 0.6 mL/min. This variation is conducive to regulating the flow rate ratio of the inner and outer phases, which can optimize the structure of hydrogel fibers and the rate of the cross-linking reaction.

The outer phase was a 3% sodium alginate solution, in which 5% lithium chloride was added as an ionic conductive dopant to enhance the electrical conductivity of the hydrogel. The outer phase was stably extruded at a constant flow rate of 0.6 mL/min using a microinjection pump. During the printing process, the inner phase flow rate changed periodically in segments in accordance with the preset program, ensuring the precise control of the hydrogel structure. The extruded hydrogel fibers were deposited in a receiving bath to complete preliminary shaping, and then solidified in the receiving bath for a certain period of time through the cross-linking reaction, so as to further improve the structural stability of the hydrogel.

4. EXPERIMENTAL RESULTS AND DISCUSSION

4.1. Influence Law of Flow Rate on the Formation of Heterotypic Lumen Hydrogel Sensors

As shown in Figure 3, a, b, and c correspond to the morphological images of hydrogel structures prepared under the step change conditions of calcium chloride flow rates of 0.7–0.6–0.7 mL/min, 0.8–0.6–0.8 mL/min, and 0.9–0.6–0.9 mL/min, respectively. With the sodium alginate flow rate kept constant, the $CaCl_2$ flow rate was only slightly adjusted around 0.6 mL/min. It can be observed that the inner diameter of the obtained hydrogel did not change significantly, no obvious shrinkage or expansion occurred between different stages, and the overall structure remained relatively stable. Within this flow rate range, the response sensitivity of the hydrogel inner diameter to changes in $CaCl_2$ flow rate was low, and the system was in a relatively stable geometric control region.

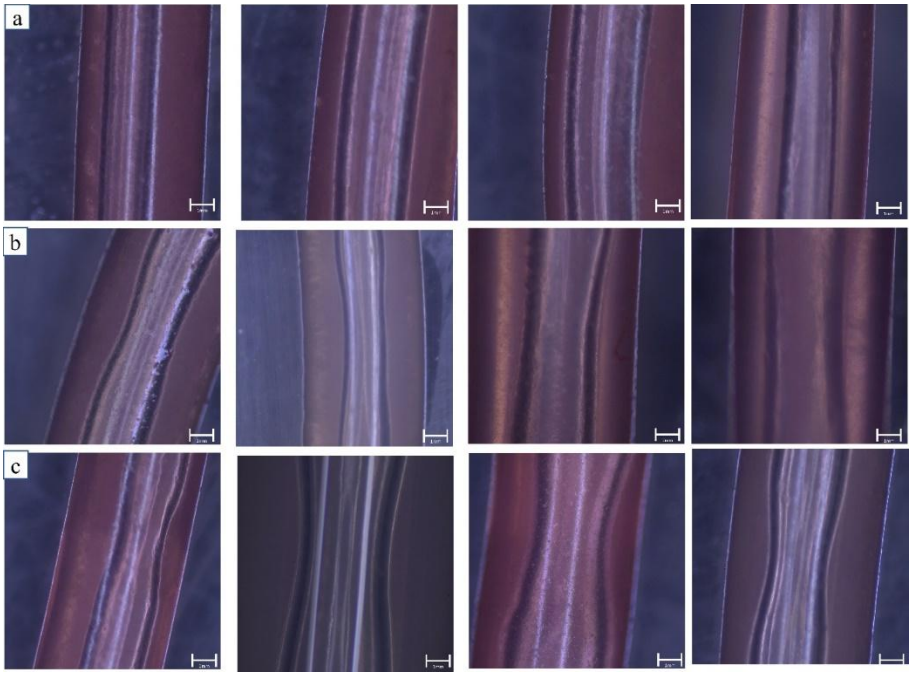

Figure 3. (a) Hydrogel Prepared at a Flow Rate of 0.7–0.6–0.7 mL/min (b) Hydrogel Prepared at a Flow Rate of 0.8–0.6–0.8 mL/min (c) Hydrogel Prepared at a Flow Rate of 0.9–0.6–0.9 mL/min

As shown in Figure 4, a and b correspond to the internal structure and morphology images of hydrogels prepared under the flow rate change conditions of calcium chloride at 1.0–0.6–1.0 mL/min and 1.1–0.6–1.1 mL/min, respectively. With the sodium alginate flow rate kept unchanged, the $CaCl_2$ flow rate was adjusted over a wide range. It can be observed that the inner diameter of the obtained hydrogel changed significantly, with obvious shrinkage and expansion between different stages, while the overall structure remained relatively stable. Within this flow rate range, the response sensitivity of the hydrogel inner diameter to changes in $CaCl_2$ flow rate was high, enabling the stable formation of internal cavities with regularly changing core lumens.

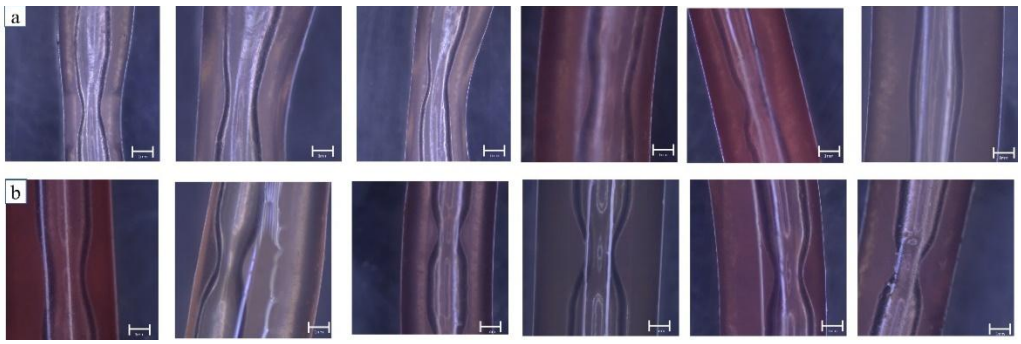

Figure 4. (a) Hydrogel Prepared at a Flow Rate of 1.0–0.6–1.0 mL/min (b) Hydrogel Prepared at a Flow Rate of 1.1–0.6–1.1 mL/min

To quantitatively analyze the influence law of $CaCl_2$ flow rate on the inner diameter, fitting analysis was performed on the data of the high flow rate stage.

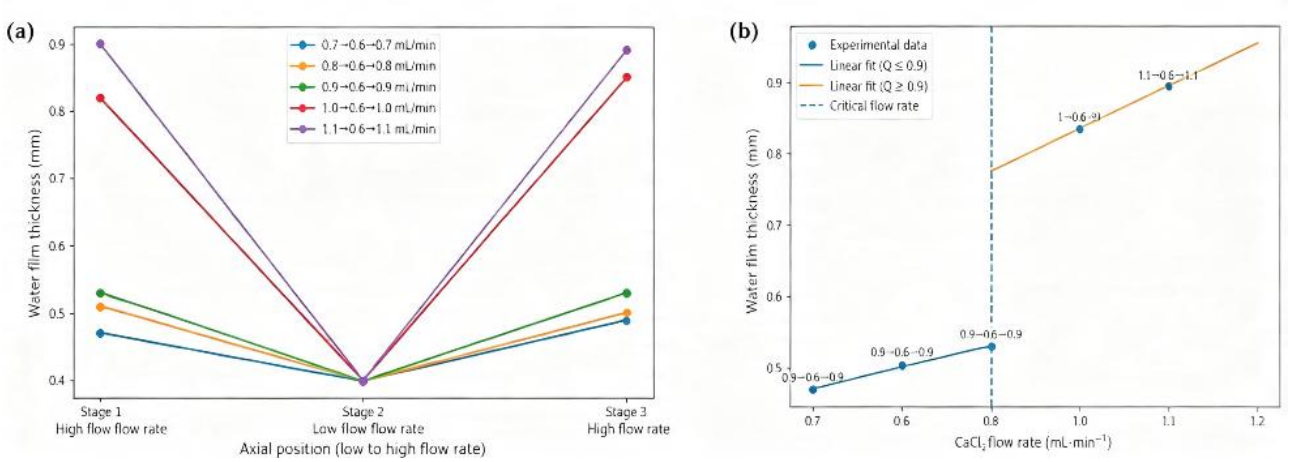

Figure 5. (a) Axial Inner Diameter Distribution of Hydrogel Lumen Under Three-Stage $CaCl_2$ Flow Rate Changes (b) Influence of $CaCl_2$ Flow Rate on Hydrogel Inner Diameter

During the experiment, the sodium alginate (SA) flow rate was fixed at 0.4 mL/min, while the $CaCl_2$ solution flow rate was adjusted to achieve a three-stage change ($Q_1 \rightarrow 0.6 \rightarrow Q_1$). The high flow rate stage Q_1 was set to 0.7, 0.8, 0.9, 1.0, and 1.1 mL/min, respectively. The hydrogel lumen inner diameter at each stage was measured via industrial microscope imaging, and its variation law was analyzed.

Figure 5(a) presents the axial inner diameter distribution of the hydrogel lumen under different $CaCl_2$ flow rates. At Stage 2 ($CaCl_2$ flow rate = 0.6 mL/min), the inner diameter of all groups was stably maintained at ~0.412 mm, indicating a stable laminar flow interface and ion diffusion equilibrium in the reaction system under low flow rate, with good repeatability of gel lumen size.

In Stages 1 and 3 (high flow rate stages, Figure 5(b)), the hydrogel inner diameter increased with increasing $CaCl_2$ flow rate. When Q_1 increased from 0.7 to 0.9 mL/min, the lumen inner diameter rose from ~0.47 to 0.53 mm; further increasing Q_1 to 1.0 and 1.1 mL/min led to a significant increase in inner diameter, reaching ~0.83 and 0.90 mm, respectively. This confirms that the high-stage $CaCl_2$ flow rate is a key parameter affecting hydrogel lumen size.

To further quantitatively analyze the effect of $CaCl_2$ flow rate on hydrogel inner diameter, the average inner diameter of Stages 1 and 3 was taken as the inner diameter of the high flow rate stage:

$$D_{high} = \frac{D_1 + D_3}{2} \tag{5}$$

Experimental Data:

Table 1. Changes in Core Inner Diameter Under Different Calcium Chloride Flow Rates

Calcium Chloride Flow Rate (ml/min)	0.6	0.7	0.8	0.9	1	1.1
mean inner diameter in the high-velocity zone (mm)	0.412	0.480	0.505	0.53	0.835	0.893

As shown in Figure 5(b), when the flow rate of $CaCl_2$ is lower than 0.9 mL/min, the lumen inner diameter of the hydrogel exhibits a slow linear increase with the flow rate, and its fitting expression is given as follows:

$$D = 0.25Q + 0.305 \tag{6}$$

Where D represents the hydrogel lumen inner diameter (mm) and Q denotes the $CaCl_2$ flow rate (mL/min).

Above 1.0 mL/min, the growth rate of the inner diameter increases markedly, with the linear fitting relation given by:

$$D = 0.60Q + 0.235 \tag{7}$$

Can be seen that the growth slope of the diameter in the high-flow velocity region is approximately 2.4 times that in the low-flow velocity region, indicating that the hydrogel lumen size is more sensitive to changes in flow rate under relatively high flow rate conditions.

Combined with the axial distribution diagram, it can be found that the three-stage flow rate changes form a stable axial structure:

$$[D_1, D_2, D_3] \approx [D_{high}, 0.40, D_{high}] \tag{8}$$

Where: D_1 is the inner diameter of Stage 1, D_2 is the inner diameter of Stage 2, and \(D_3\) is the inner diameter of Stage 3.

The inner diameter of Stage 2 remains basically constant:

$$D_2 \approx 0.40mm \tag{9}$$

In contrast, the inner diameters of Stage 1 and Stage 3 are determined by the high-flow velocity region function $D_{high}(Q)$.

4.2. Mechanical and Electrical Performance Analysis of Hydrogel Sensors for Irregular Luminal Structures

It can be seen from Figure 6(a) that as the sodium alginate concentration gradually increases from 3% to 5%, both the tensile strength and elongation at break of the hydrogel increase correspondingly. A higher sodium alginate concentration leads to a gradual steepening of the stress-strain curve of the hydrogel, indicating an enhancement in the tensile strength of the hydrogel. The increase in sodium alginate concentration increases the concentration of polymer chains, resulting in tighter ionic cross-linking between Ca^{2+} and sodium alginate. This dense cross-linked structure endows the hydrogel with stronger mechanical properties, especially a significant improvement in stress resistance. With the increase of sodium alginate concentration, the network structure of the hydrogel becomes more compact, exhibiting a higher maximum elongation. In the high-concentration sodium alginate hydrogel, the network structure can be stretched more effectively under stress, which enhances the toughness of the material.

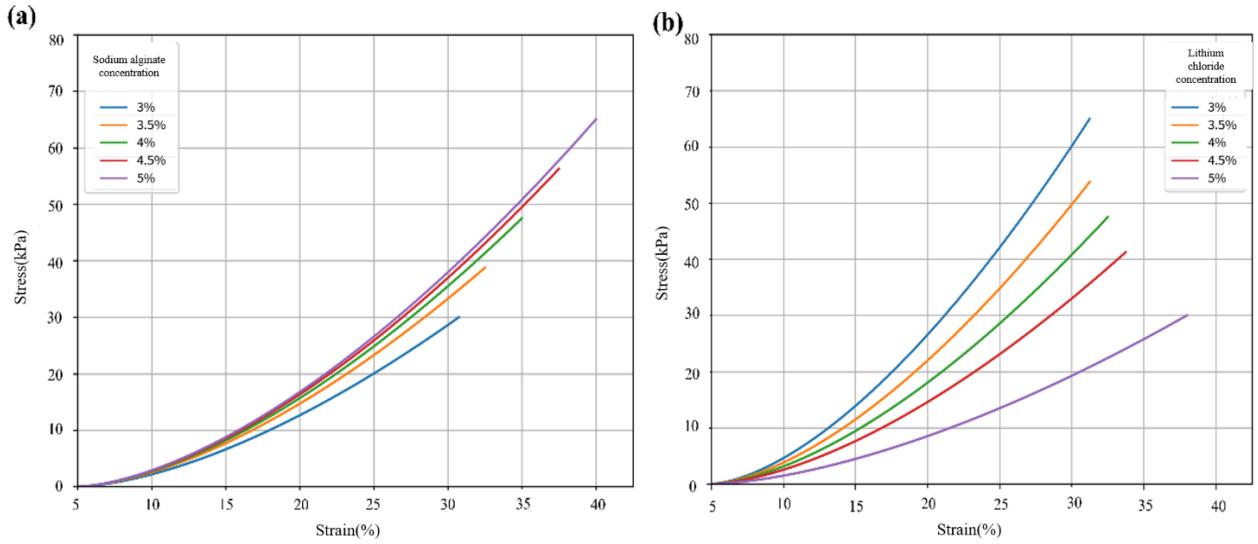

Figure 6. Effects of different sodium alginate and lithium chloride concentrations on hydrogel properties (a) Effect of sodium alginate concentration on hydrogel tensile properties (b) Effect of lithium chloride concentration on hydrogel tensile properties

As shown in Figure 6(b), when lithium chloride (LiCl) concentration increases from 3% to 5%, the hydrogel's tensile strength decreases continuously (maximum stress from 65 kPa to 30 kPa), while strain increases from 32% to 37%, indicating improved elongation. Mechanistically, higher LiCl concentration enhances Li^{+}-mediated charge shielding on carboxyl groups, weakening ionic cross-linking between Ca^{2+} and sodium alginate (SA). This loosens the hydrogel's internal network, reducing tensile strength but decreasing cross-link rigidity to improve flexibility and elongation under stress.

Overall, hydrogel plasticity increases with LiCl concentration, enabling it to withstand greater strain without fracture. Notably, as LiCl concentration rises from 3% to 5%, the stress-strain curve's change rate accelerates—high LiCl concentrations allow the hydrogel to generate large stress even under small strain, attributed to looser network structure and reduced ion migration resistance enhancing stress response speed.

To explore SA and LiCl concentration effects on hydrogel conductivity, tests were conducted under different concentrations (results in Figure 7(a) and (b)), showing both components significantly affect conductivity with distinct variation rules.

SA concentration exerts a non-linear effect on conductivity: increasing from 3% to 3.75% raises conductivity from 30.2 S/m to 33.43 S/m, while further increasing to 5% decreases it to 26.33 S/m, with a maximum of 33.43 S/m at 3.75%.

In contrast, LiCl concentration shows a stable increasing effect: conductivity rises from 31.12 S/m to 33.86 S/m as LiCl increases from 3% to 5%, with a near-linear continuous upward trend throughout the experimental range.

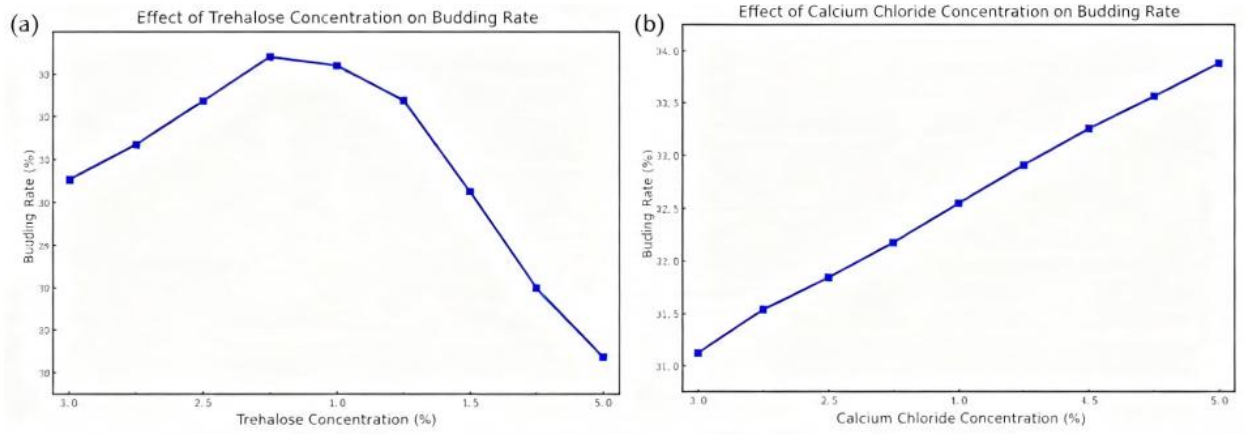

Figure 7. (a) Effect of sodium alginate (SA) concentration on the conductivity; (b) Effect of lithium chloride (LiCl) concentration on the conductivity

Comparison of the two sets of experimental results shows that sodium alginate (SA) concentration exhibits an obvious optimal concentration effect on electrical conductivity, while lithium chloride (LiCl) concentration mainly enhances conductivity by increasing ionic concentration.

SA, a natural polysaccharide polymer with abundant hydrophilic groups ($–COO^-$ and –OH), forms a three-dimensional network in aqueous solution, affecting ion migration and conductivity. At low SA concentrations, increasing SA content raises polymer chain and mobile ion numbers; the loose chain structure ensures low ion migration resistance, steadily improving conductivity. When SA concentration reaches 3.75 wt%, the polymer network and ionic concentration reach balance, providing a stable ion transport environment, thus maximizing ionic transport efficiency and achieving a peak conductivity of 34.26 S/m.

Within the studied range, LiCl concentration does not reach the critical value for significant ion–ion interactions, so ion migration is unimpeded, and system conductivity increases continuously.

Consistent with previous studies, polymer electrolyte conductivity is regulated by ionic concentration, solution viscosity, and polymer chain structure: conductivity increases with low polymer concentration but decreases when concentration exceeds a threshold due to increased viscosity and chain entanglement. This study's SA concentration effect on conductivity aligns with this conclusion, showing a distinct optimal point. Meanwhile, LiCl, as an excellent ion-dissociating lithium salt, enhances system ionic transport, and its concentration-dependent conductivity trend is consistent with relevant literatures.

In summary, both SA and LiCl concentrations significantly affect conductivity: SA concentration leads to a first increase and then decrease in conductivity (maximum 33.43 S/m at 3.75 wt%), while LiCl concentration results in continuous conductivity increase (33.86 S/m at 5 wt% within the experimental range).

To explore the hydrogel's electrical response during stretching, uniaxial tensile resistance tests were conducted. The hydrogel (initial length 3 cm) was stretched to 4.2 cm (strain 0–40%), with real-time resistance recording to obtain electrical response data under different strains. Resistance–strain, relative resistance change, and gauge factor curves were plotted to systematically evaluate strain-sensing performance.

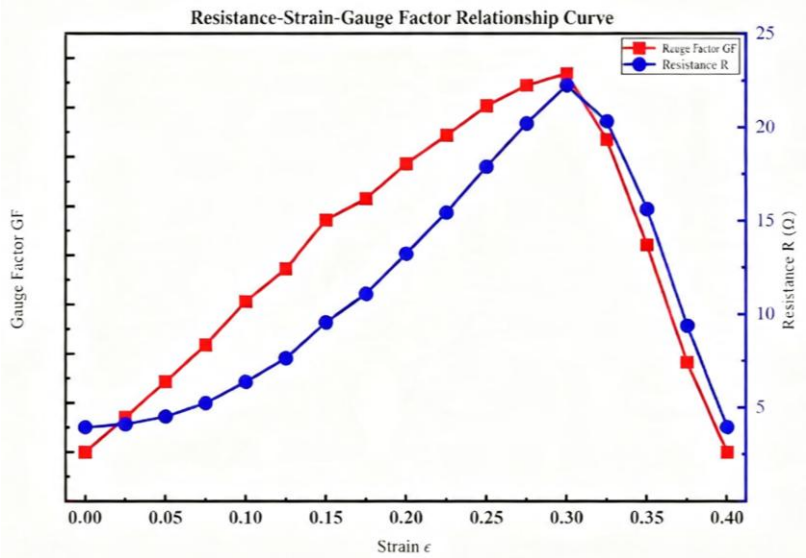

Figure 8. Relationship between Resistance, Strain, and Sensitivity

Table 2. Effect of Strain on Resistance

Strain (%)	Resistance (kΩ)		
0	3.92	3.94	4.1
0.025	4.04	4.11	4.15
0.05	4.46	4.51	4.59
0.075	5.16	5.27	5.3
0.1	6.27	6.41	6.43
0.125	7.54	7.68	7.71
0.15	9.42	9.59	9.64
0.175	10.93	11.15	11.19
0.2	13.06	13.29	13.34
0.225	15.22	15.49	15.55
0.25	17.65	17.96	18.01
0.275	19.94	20.27	20.33
0.3	21.93	22.3	22.37
0.325	20.07	20.38	20.45
0.350	15.42	15.68	15.74
0.375	9.25	9.4	9.46
0.4	0	0	0

As shown in Figures 8, the hydrogel's resistance increases gradually with strain: its initial resistance is 3.96 kΩ, rising to 22.24 kΩ at 30% strain, indicating a positive correlation between resistance change and strain due to significant alterations in the internal conductive network during stretching. In the low strain range (0–10%), resistance changes gently with low sensitivity; beyond this range, the resistance change rate accelerates, especially above 30% strain, where the conductive paths and core structure undergo obvious changes.

Figure 8 shows that $\Delta R/R_0$ increases from 0 to 4.61 with strain, further verifying the non-linear positive correlation between hydrogel resistance and strain, and the accelerated relative resistance change above 30% strain indicates significant damage to the conductive network, endowing the hydrogel with high sensing sensitivity in the large strain range.

Figure 8 illustrates the variation of hydrogel sensitivity (GF) with strain: GF increases in 0–10% strain, reaching a maximum of 15.39 at 30% strain. Mechanistically, stretching deforms the hydrogel's three-dimensional network, lengthening conductive ion migration paths and reducing conductive channels, while the irregular luminal structure enhances geometric deformation and ion transport path changes, thus improving resistance response sensitivity.

Beyond 30% strain, GF gradually decreases due to conductive network damage and reduced contact between conductive fillers. The hydrogel fractures at 40% strain (stretched to 4.2 cm), with a sharp increase in resistance and GF dropping to 0, losing strain sensing function, indicating limited structural stability under large deformation.

The hydrogel's strain sensing performance relies on internal conductive network changes: stable paths without external force, increased filler distance and damaged paths (thus increased resistance) under stretching, with aggravated network damage and improved sensitivity as strain increases (maximum sensitivity at 30% strain). Further stretching destabilizes the network and reduces sensitivity, with complete failure at the 40% fracture point.

Comparison with reported hydrogel strain sensors shows that traditional ion-conductive hydrogels have a GF of 1–10, while structural optimization or composite fillers can increase GF to 10–50 or higher. The prepared irregular luminal hydrogel has a GF of 15.39, significantly higher than ordinary ion hydrogels, demonstrating the advantage of the irregular luminal structure

4.3. Discussion

This study systematically investigated the effects of reactant concentration, solution flow rate and co-flow distance on the crosslinking layer thickness, average reaction rate and related properties of hydrogels. Through experimental testing, data fitting and mechanism analysis, the action rules of various factors were clarified, providing experimental basis and theoretical support for the structural regulation and performance optimization of hydrogels.

The concentrations of sodium alginate and lithium chloride jointly affect the mechanical properties and electrical conductivity of the hydrogel. The increase of sodium alginate concentration can enhance the tightness of ionic crosslinking and improve the tensile strength and elongation at break of the hydrogel; the increase of lithium chloride concentration weakens the crosslinking effect through the charge shielding effect, reduces the tensile strength but improves the elongation performance. In terms of electrical conductivity, the sodium alginate concentration shows a trend of first increasing and then decreasing, reaching a maximum value of 33.43 S/m at 3.75%; the lithium chloride concentration increases continuously and linearly with the increase of concentration, and the electrical conductivity reaches 33.86 S/m at 5%. The optimal ratio is 3.8% sodium alginate and 5% lithium chloride.

The hydrogel has good strain sensing performance. When the strain is 0–30%, the resistance and relative resistance increase non-linearly with strain, and the gauge factor (GF) reaches a maximum value of 15.39 at 30% strain, which is higher than that of ordinary ion hydrogel sensors; after the strain exceeds 30%, the sensitivity attenuates, and the hydrogel breaks at 40%, losing the sensing function.

5. CONCLUSIONS

Aiming at the problem of poor adjustability of mechanical and electrical properties of hydrogel sensors prepared by coaxial reaction flow method, this study systematically investigated the design, preparation, performance testing and application potential of irregular luminal hydrogel sensors. Through experimental exploration and theoretical analysis, the key problems of precise regulation

and performance optimization of irregular luminal structure were solved, and the main conclusions are as follows:

(1) A precise and controllable preparation platform for irregular luminal hydrogels was successfully built. By improving the coaxial nozzle structure, optimizing the fluid control system, and combining the segmented flow rate control strategy, the continuous and stable preparation of variable-diameter irregular luminal hydrogels was realized. The proposed flow rate control theoretical model can effectively predict the changes of lumen morphology, providing theoretical support for structural optimization.

(2) The regulation rule of $CaCl_2$ flow rate on the morphology of irregular luminal was clarified, with an obvious flow rate threshold effect. When the flow rate is 0.6–0.9 mL/min, the inner diameter of the lumen changes gently and the system is stable; when the flow rate is ≥1.0 mL/min, the inner diameter increases significantly and is sensitive to flow rate response. The slope of inner diameter growth in the high flow rate region is 2.4 times that in the low flow rate region, and the precise control of lumen size can be realized by adjusting the flow rate.

(3) The optimal concentration ratio of sodium alginate and lithium chloride was determined. The increase of sodium alginate concentration can enhance the tightness of crosslinking and improve the mechanical properties; the increase of lithium chloride concentration weakens the crosslinking effect, reduces the tensile strength but improves the elongation performance and conductivity. When the ratio of sodium alginate to lithium chloride is 3.75% and 5%, the hydrogel has the best comprehensive performance, with a maximum stress of 65 kPa and an electrical conductivity of 33.86 S/m.

In summary, this study realized the precise regulation of the structure and performance of irregular luminal hydrogels through flow rate regulation and concentration optimization, solved the problem of poor performance adjustability of traditional hydrogel sensors, and provided strong theoretical and practical support for their applications in high-precision biological signal monitoring, flexible electronic devices and other fields.

REFERENCES

[1] Sakai S, Liu Y, Mah E J, et al. Horseradish peroxidase/catalase-mediated cell-laden alginate-based hydrogel tube production in two-phase coaxial flow of aqueous solutions for filament-like tissues fabrication [J]. Biofabrication, 2013, 5(1): 015012.

[2] Blaeser A, Million N, Campos D F D, et al. Laser-based in situ embedding of metal nanoparticles into bioextruded alginate hydrogel tubes enhances human endothelial cell adhesion [J]. Nano Research, 2016, 9: 3407-3427.

[3] Torres-Rendon J G, Köpf M, Gehlen D, et al. Cellulose nanofibril hydrogel tubes as sacrificial templates for freestanding tubular cell constructs [J]. Biomacromolecules, 2016, 17(3): 905-913.

[4] Liu L, Wang N, Han Y, et al. Redox-triggered self-rolling robust hydrogel tubes for cell encapsulation [J]. Macromolecular rapid communications, 2014, 35(3): 344-349.

[5] Xu B, Li Y, Gao F, et al. High strength multifunctional multiwalled hydrogel tubes: ion-triggered shape memory, antibacterial, and anti-inflammatory efficacies [J]. ACS applied materials & interfaces, 2015, 7(30): 16865-16872.

[6] Xu P, Xie R, Liu Y, et al. Bioinspired microfibers with embedded perfusable helical channels [J]. Advanced Materials, 2017, 29(34): 1701664.

[7] Yu Y, Fu F, Shang L, et al. Bioinspired helical microfibers from microfluidics [J]. Advanced Materials, 2017, 29(18): 1605765.

[8] Cheng Y, Zhang X, Cao Y, et al. Centrifugal microfluidics for ultra-rapid fabrication of versatile hydrogel microcarriers [J]. Applied Materials Today, 2018, 13: 116-125.

[9] Xie R, Xu P, Liu Y, et al. Necklace-like microfibers with variable knots and perfusable channels fabricated by an oil-free microfluidic spinning process [J]. Advanced Materials, 2018, 30(14): 1705082.

[10] Wu B, Jian Y, Le X, et al. Supramolecular fabrication of complex 3d hollow polymeric hydrogels with shape and function diversity [J]. ACS applied materials & interfaces, 2019, 11(51): 48564-48573.

[11] Liang S, Tu Y, Chen Q, et al. Microscopic hollow hydrogel springs, necklaces and ladders: a tubular robot as a potential vascular scavenger [J]. Materials Horizons, 2019, 6(10): 2135-2142.

[12] Liang S, Tu Y, Chen Q, et al. Microscopic hollow hydrogel springs, necklaces and ladders: a tubular robot as a potential vascular scavenger [J]. Materials Horizons, 2019, 6(10): 2135-2142.

[13] Jia L, Han F, Yang H, et al. Microfluidic fabrication of biomimetic helical hydrogel microfibers for blood-vessel-on-a-chip applications [J]. Advanced healthcare materials, 2019, 8(13): 1900435.

[14] Liu R, Kong B, Chen Y, et al. Formation of helical alginate microfibers using different G/M ratios of sodium alginate based on microfluidics [J]. Sensors and Actuators B: Chemical, 2020, 304: 127069.

[15] Dolati F, Yu Y, Zhang Y, et al. In vitro evaluation of carbon-nanotube-reinforced bioprintable vascular conduits [J]. Nanotechnology, 2014, 25(14): 145101.

[16] Zhang Y, Yu Y, Chen H, et al. Characterization of printable cellular micro-fluidic channels for tissue engineering [J]. Biofabrication, 2013, 5(2): 025004.22

[17] Hua M, Wu S, Ma Y, et al. Strong tough hydrogels via the synergy of freeze-casting and salting out [J]. Nature, 2021, 590(7847): 594-599.

[18] Yu Y, Zhang Y, Martin JA, et al. Evaluation of cell viability and functionality in vessel-like bioprintable cell-laden tubular channels [J]. J Biomech Eng, 2013, 135(9): 91011.